



Evaluation of multi-phase atmospheric dispersion models for application to Carbon Capture and Storage



S.E. Gant^{a,*}, V.D. Narasimhamurthy^b, T. Skjold^b, D. Jamois^c, C. Proust^{c,d}

^a Health and Safety Laboratory (HSL), Harpur Hill, Buxton SK17 9JN, UK

^b GexCon A.S., P. O. Box 6015, NO-5892, Bergen, Norway

^c INERIS, Dept. PHDS, Parc Technologique ALATA, BP 2, 60550 Verneuil-en-Halatte, France

^d UTC Laboratoire TIMR EA4297, Centre Pierre Guillaumat, 60200 Compiègne, France

ARTICLE INFO

Article history:

Received 18 June 2014

Received in revised form

26 September 2014

Accepted 26 September 2014

Available online 30 September 2014

Keywords:

CCS

Carbon dioxide

Dispersion

Phast

CFD

ABSTRACT

A dispersion model validation study is presented for atmospheric releases of dense-phase carbon dioxide (CO₂). Predictions from an integral model and two different Computational Fluid Dynamics (CFD) models are compared to data from field-scale experiments conducted by INERIS, as part of the EU-funded CO₂PipeHaz project.

The experiments studied consist of a 2 m³ vessel fitted with a short pipe, from which CO₂ was discharged into the atmosphere through either a 6 mm or 25 mm diameter orifice. Comparisons are made to measured temperatures and concentrations in the multi-phase CO₂ jets.

The integral dispersion model tested is DNV Phast and the two CFD models are ANSYS-CFX and a research and development version of FLACS, both of which adopt a Lagrangian particle-tracking approach to simulate the sublimating solid CO₂ particles in the jet. Source conditions for the CFD models are taken from a sophisticated near-field CFD model developed by the University of Leeds that simulates the multi-phase, compressible flow in the expansion region of the CO₂ jet, close to the orifice.

Overall, the predicted concentrations from the various models are found to be in reasonable agreement with the measurements, but generally in poorer agreement than has been reported previously for similar dispersion models in other dense-phase CO₂ release experiments. The ANSYS-CFX model is shown to be sensitive to the way in which the source conditions are prescribed, while FLACS shows some sensitivity to the solid CO₂ particle size. Difficulties in interpreting the results from one of the tests, which featured some time-varying phenomena, are also discussed.

The study provides useful insight into the coupling of near- and far-field dispersion models, and the strengths and weaknesses of different modelling approaches. These findings contribute to the assessment of potential hazards presented by Carbon Capture and Storage (CCS) infrastructure.

Crown Copyright © 2014 Published by Elsevier Ltd. This is an open access article under the CC BY-NC-SA license (<http://creativecommons.org/licenses/by-nc-sa/3.0/>).

1. Introduction

The introduction of CCS will result in CO₂ being produced and transported in much greater quantities than it is today. It has been estimated that in order to generate 1 GW of electrical power from a coal-fired power station fitted with CCS will require around

30,000 tonnes/day of CO₂ to be captured and sequestered into long-term storage facilities (Harper, 2011).

To transport CO₂ from emitters, such as power stations, to sequestration sites, it is likely that pipelines will be used that will operate with the CO₂ in a dense-phase state, as either a supercritical fluid or liquid, i.e. at a pressure higher than 74 barg, and a temperature above or below its critical temperature of 31 °C. As part of the design and risk assessment process for CCS infrastructure, an understanding is required of the consequences of an intentional or accidental release of dense-phase CO₂.

When dense-phase CO₂ is discharged into the atmosphere, it is transformed into a mixture of gaseous and solid CO₂ (dry ice) at ambient temperature and pressure. The drop in pressure from the

* Corresponding author.

E-mail addresses: simon.gant@hsl.gsi.gov.uk (S.E. Gant), vagesh.d.narasimhamurthy@gexcon.com (V.D. Narasimhamurthy), trygve@gexcon.com (T. Skjold), didier.jamois@ineris.fr (D. Jamois), christophe.proust@ineris.fr (C. Proust).

operating conditions to atmospheric pressure is also accompanied by significant cooling, since CO₂ has a high Joule–Thomson effect. For CO₂ at saturation conditions of 300 K and 67 bar, the Joule–Thomson coefficient is approximately 0.9 K/bar (Perry, 2007). In comparison, for nitrogen at a similar temperature and pressure, the Joule–Thomson coefficient is slightly negative at around –0.01 K/bar. The positive coefficient value for CO₂ indicates a reduction in temperature with pressure, whereas the small negative value for nitrogen indicates a slight increase in temperature with falling pressure.

This unusual release behaviour of CO₂ presents a number of challenges for dispersion models that are used to predict the extent of the toxic cloud. This paper provides a review of the recent research in this area, followed by a description of the experiments, modelling and results of the validation exercise that was conducted as part of the EU-funded CO₂ PipeHaz project.¹

2. Review of related research

Over the last decade, there have been a number of major research projects directed towards understanding the new safety issues presented by industrial-scale CCS. Perhaps the earliest study looking specifically at validation of dense-phase CO₂ dispersion models was undertaken in support of BP's Decarbonised Fuels 1 (DF1) project, in which it was planned to capture CO₂ emitted from the Peterhead power station in the UK and sequester it in the Miller oilfield under the North Sea. As part of this project, experiments were conducted at the GL Noble Denton Spadeadam test site and a number of consultancies performed dispersion model predictions. Some results from the MMI Engineering contribution to that project were published by Dixon and Hasson 2007 and Dixon et al. 2009. In the first of their two papers, results were presented using the CFD code ANSYS-CFX, in which the solid CO₂ particles in the jet were modelled using a transported scalar to represent the particle concentration. This approach was taken to avoid the additional computing time associated with the alternative particle-tracking approach. However, one of its limitations was that in calculating the heat and mass exchange between the particles and the gas phase it was necessary to assume a constant particle diameter. The CO₂ gas distribution within the jet may have therefore been poorly predicted, since the sublimation rate increases as the particle size decreases in the jet. In addition, the particle temperature was assumed to remain constant at the sublimation temperature of –78 °C, i.e. a “boiling” assumption was made. In their second paper (Dixon et al., 2009), solid CO₂ particles were modelled using a Lagrangian particle-tracking approach. However, the particles were still assumed to remain at a constant temperature of –78 °C, whereas in reality the particle temperature is expected to fall in the jet, to perhaps as low as –100 °C. In both of their papers (Dixon and Hasson, 2007; Dixon et al., 2009), scales were omitted on the axes of graphs showing the comparison of model predictions against experiments, due to confidentiality of the experimental data.

E.ON have published a number of studies in support of their proposed CCS programme (Mazzoldi et al., 2008a, 2008b, 2011; Hill et al., 2011). The most relevant of these, for the present work, are by Mazzoldi et al. (2011) and Hill et al. (2011), which considered atmospheric dispersion from pipelines and vessels. The former paper compared simulations from the heavy gas model ALOHA to the CFD model Fluidyn-Panache. Although the work focused on discharges of dense-phase CO₂ from a 100 bar release, only the gaseous stage of the discharges were modelled. The bulk of the analysis consisted

of comparisons between the two models, rather than validation against experimental data.

Hill et al. (2011) presented CFD and Phast simulations of dense-phase CO₂ releases from a 0.5 m diameter hole in a pipeline, located at an elevation of 5 m above flat ground. CFD simulations were performed using the ANSYS-CFX code with a Lagrangian particle-tracking model for the solid CO₂ particles. To examine the effect of the particle size, Hill et al. (2011) performed simulations using three different particle size distributions: from 10 to 50 μm, 50 to 100 μm and 50 to 150 μm. Simulations were also performed using no solid CO₂ particles. The results showed that sublimation of the particles led to cooling of the CO₂ plume, which affected its dispersion behaviour, but the results were relatively insensitive to the particle size. Predicted gas concentrations were lower using Phast version 6.6 than with ANSYS-CFX, but there was no comparison of model predictions to experiments.

One of the differences between the ANSYS-CFX model used by Hill et al. (2011) and that used in the present study is that Hill et al. (2011) used a Lagrangian model that did not account for the effect of turbulence on the dispersion of the solid CO₂ particles. The particle tracks were not spread throughout the plume but instead followed closely the plume centreline. Ignoring turbulent dispersion effects can have a significant influence on the model predictions, particularly the temperature. Turbulence has the effect of bringing particles into contact with parts of the jet at a higher temperature and lower CO₂ concentration. This tends to increase the rate of sublimation and increase the radius of the region cooled by the sublimating particles.

DNV Software has produced several key papers on CO₂ release and dispersion modelling (Witlox et al., 2009, 2011, 2012). In the first of these, Witlox et al. (2009) described an extension to the existing model in Phast version 6.53.1 to account for the effects of solid CO₂. The modifications consisted principally of changing the way in which equilibrium conditions were calculated in the expansion of CO₂ to atmospheric pressure, to ensure that below the triple point, conditions followed the sublimation curve in the phase diagram. Furthermore, two-phase vapour/solid effects instead of vapour/liquid effects were included downstream of the orifice, after the CO₂ jet had depressurised to ambient pressure. Although the revised model was validated against experimental data, the measurements were confidential and were not reported. In the second paper (Witlox, 2010), the results of a sensitivity analysis were reported for both liquid and supercritical CO₂ releases from vessels and pipes, using the revised Phast version 6.6 model. Again, no experimental validation was presented due to data confidentiality. In more recent work (Witlox et al., 2012), results were finally compared to experimental data that was made publicly available as part of the CO₂PipeTrans joint industry project.² These experiments, which were originally funded by BP and Shell, consisted of above-ground, horizontal releases of supercritical and liquid CO₂, using orifice diameters from ¼" to 1" diameter (6.5 mm to 25.4 mm). The measured flow rates were predicted by Phast with an error of less than 10% and the dispersion model predictions were in good agreement with data (well within the factor-of-two criteria often used to assess the performance of atmospheric dispersion models).

The same Shell experiments were also modelled independently by Shell and HSL using the Shell FRED integral dispersion model, and two different CFD codes, OpenFOAM and ANSYS-CFX (Dixon et al., 2012). Both FRED (Betteridge and Roy, 2010) and the OpenFOAM models assumed Homogeneous Equilibrium (HE) between

¹ <http://www.co2pipehaz.eu>, accessed 28 January 2014.

² <http://www.dnv.com/ccs>, accessed 28 January 2014.

the CO₂ particles and the vapour phase, i.e. the particles and surrounding vapour shared the same temperature and velocity. The ANSYS-CFX model, in contrast, used a Lagrangian particle-tracking approach in which the temperature and velocity of the solids and vapour could differ, depending upon the predicted rates of heat and mass transfer between the two phases. All three models were found to provide generally good predictions of the concentrations along the centreline of the jets, although jet widths were slightly better predicted by FRED than the two CFD models. The results from the two CFD models were similar, despite the differences in their underlying physical basis, which indicated that HE is a reasonable approximation for unimpeded jet releases of that scale, when the solid CO₂ particle size is small.

TNO have undertaken various relevant studies as part of the CATO2³ and COCATE⁴ projects. In their early work, Hulsbosch-Dam et al. (2011) compared CFD model predictions using Fluent to the Phast and ANSYS-CFX dispersion model predictions previously presented by Hill et al. (2011). Significant differences were obtained between the TNO Fluent and E.ON ANSYS-CFX results. Whilst Hill et al. (2011) found that ANSYS-CFX predicted higher concentrations than Phast, Hulsbosch-Dam et al. (2011) found that Fluent predicted lower values. This behaviour was attributed to differences in the implementation of neutral atmospheric boundary layers and the solid CO₂ particle size in the two CFD codes. Subsequently, Hulsbosch-Dam et al. (2012) developed a semi-empirical model for the solid CO₂ particle size distribution in CO₂ jets, which they validated using experimental data for CO₂ and other superheated liquids. For initial pressures of between 40 bar and 100 bar, and temperatures of between -10 °C and 30 °C, their model predicted the Sauter mean diameter of the CO₂ particles to be between 1 µm and 20 µm. The authors noted that for horizontal CO₂ jet releases, such small particles would probably sublimate within the jet, rather than rain-out, although some deposition of solid CO₂ could occur if the jet impinged on a nearby surface.

The influence of the atmospheric boundary layer and terrain on CO₂ dispersion was investigated further at TNO by Mack and Spruijt (2013a, 2013b), who first validated their OpenFOAM CFD model using data from the Hamburg wind tunnel dispersion experiments and the field-scale Desert Tortoise tests, taken from the REDIPHEN database (Nielsen and Ott, 1995), before going on to simulate a large-scale gaseous CO₂ release over complex terrain. The results from these final simulations showed that differences in terrain heights of 53 m (from the highest to the lowest point) had an appreciable effect on the dispersion behaviour of the CO₂ in low wind speeds of 3 m/s, but only a minor influence in high wind speeds of 12 m/s to 16 m/s. As part of the CATO2 project, DNV KEMA and TNO have also recently performed a series of laboratory-based dense-phase CO₂ release experiments (Ahmad et al., 2013a, 2013b), which should provide a useful dataset for future model validation.

The ongoing National Grid COOLTRANS project is probably the most extensive of the current projects aimed at validating dispersion models for dense-phase CO₂ pipeline releases. As part of this project, a comprehensive series of experiments has been conducted at Spadeadam, which has included a series of up to 2" (50.8 mm) diameter vent releases, 144 m long, 6" (150 mm) diameter shock-tube releases, and both punctures and ruptures of buried pipelines (Cooper, 2012). As part of this project, University College London (UCL) has developed models for pipeline depressurization and outflow (Mahgerfeh et al., 2012), the University of Leeds have developed models for near-field dispersion (Wareing et al., 2013) and Kingston University have developed models for far-field

dispersion (Wen et al., 2013). The same models developed by UCL and University of Leeds are used to provide upstream boundary conditions for the simulations shown in the present paper. As part of the COOLTRANS project, GL Noble Denton is also in the process of developing a semi-empirical source model for releases from pipeline craters (Cleaver et al., 2013) and HSL is preparing a model evaluation protocol for dense-phase CO₂ dispersion models (Gant, 2012).

At HSL, small-scale experiments are currently in progress to examine the dispersion behaviour of gaseous and liquid CO₂ releases under well-controlled laboratory conditions. Preliminary results from these experiments have been presented by Pursell (2012). In addition, Webber (2011) presented a methodology for extending existing two-phase homogeneous equilibrium integral models for flashing jets to the three-phase case for CO₂, and Gant and Kelsey (2012) examined the effect of concentration fluctuations in gaseous releases of CO₂ on the toxic load. The sensitivity of Phast model predictions to various input conditions for the case of a horizontal dense-phase CO₂ jet releases was examined by Gant et al. (2013). In their study, seven model inputs were varied: the vessel temperature and pressure, orifice size, wind speed, humidity, ground surface roughness and height of the release. The analysis showed that the orifice size and release height had the greatest influence on the dispersion distance, across the particular range of conditions that were tested.

In addition to the above research, dense-phase CO₂ releases continue to be studied for the CO₂PipeTrans and COSHER⁵ projects.

The contribution of the present work to the ongoing research effort in this field is a validation study in which three different CO₂ dispersion models are compared against experimental data produced recently as part of the EU-funded CO₂PipeHaz project. The key difference of this work, as compared to the previous studies, is that the far-field dispersion models tested here use very detailed source conditions that are taken from solutions of the complex near-field flow, which were produced by the University of Leeds (Woolley et al., 2013). In the various studies reviewed above, integrated source conditions (i.e. simple top-hat shaped profiles) have been used instead. In the analysis presented below, two different techniques for coupling the near- and far-field models are tested and the strengths and weakness of different underlying model assumptions are investigated.

3. Experimental arrangement

The apparatus that was used in the INERIS experiments is shown in Fig. 1. Liquid CO₂ was stored in an insulated 2 m³ vessel, mounted on load cells that recorded the weight of the vessel to an accuracy of ±0.5 kg. The mass flow rate from the vessel was calculated by taking the time-derivative of the recorded mass, and this method was estimated to have an accuracy of ±0.2 kg/s. The liquid take off from the vessel was via a 50 mm diameter pipe with a total length of 6.3 m (including the length of pipe both inside and outside the vessel). This was fitted with two balls valves: a manual isolation valve and a remote-actuated control valve, which both offered very low flow resistance. Inside the vessel was a vertical rake of six K-type thermocouples (with an accuracy of ±0.25 °C), which were located on the central axis of the vessel. An additional thermocouple was mounted within the orifice plate at the end of the pipe. KISTLER piezoresistive pressure transducers with an accuracy of ±0.1 bar were used to record the pressure inside the vessel. The pressure was also measured at a position immediately upstream of the orifice using a KULITE transducer with an accuracy of ±3 bar.

³ <http://www.co2-cato.org/>, accessed 28 January 2014.

⁴ http://projet.ifpen.fr/Projet/jcms/c_7861/cocate, accessed 28 January 2014.

⁵ <http://www.dnvkema.com/innovations/ccs/transport-research/default.aspx>, accessed 28 January 2014.

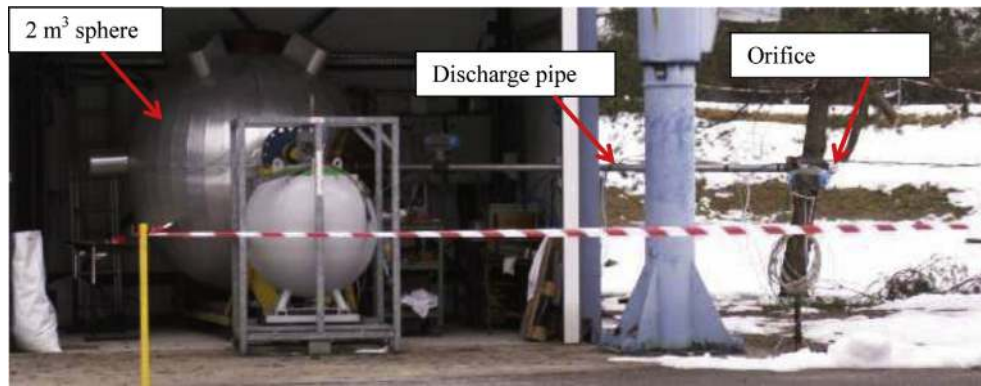


Fig. 1. INERIS experimental arrangement.

The CO₂ was discharged into an open test pad with instruments mounted on masts at various positions along the axis of the jet, as shown in Fig. 2.

In total, 13 tests were conducted using this apparatus, which were reported (in French) by Jamois et al. (2013). The present work focuses on just two of them: Tests 2 and 8. In Test 2, the thermocouples were located along the axis of the CO₂ jet at five locations 1 m apart, from 1 m to 5 m from the orifice. Concentrations of CO₂ were inferred from SERVOMEX paramagnetic oxygen sensors at three positions along the axis of the jet, at 1 m, 3 m and 5 m from the orifice. A different arrangement of thermocouples was used in the jet for Test 8, in which temperatures were recorded at various different heights on six masts that were spaced apart along the axis of the jet at distances of at 1 m, 2 m, 5 m, 10 m, 20 m and 37 m. Thermocouples were also mounted on four masts arranged at right-angles to the axis of the jet, to measure the width of the cloud at a distance of 20 m from the orifice. Oxygen concentrations were measured along the axis of the jet on each of the six masts.

In both Tests 2 and 8, the thermocouples used to measure temperatures in the plume had a diameter of 0.5 mm and a response time of less than a second. Type K thermocouples were selected for their sensitivity in the range of the observations, which was better than other types of thermocouples with the exception of Type T (which was not available in sheathed form with small diameters of 0.5 mm). The releases were also recorded on video using both Infra-Red (IR) and visual cameras.

The estimated measurement uncertainty in the recorded CO₂ concentrations, which were calculated from the oxygen sensor data, was less than $\pm 1\%$ v/v CO₂. It was shown by Jamois et al. (2013) that these derived CO₂ concentrations were within 1% v/v of the concentrations inferred from the temperature data. However, to determine concentrations from temperatures requires prior knowledge of the CO₂ liquid fraction at the orifice – which was not measured. The approach taken by Jamois et al. (2013) was to infer the value of the liquid mass fraction from the temperature and concentration data that were both measured at one position, and then to use this value to calculate the concentrations elsewhere in the jet. In the present paper, only the concentration data from the oxygen cell measurements is shown.

The conditions present during Tests 2 and 8 are summarised in Table 1. All of the tests were conducted in a local wind speed of less than 0.1 m/s, in order to avoid the wind affecting the dispersion behaviour of the CO₂ cloud. Fig. 3 shows the measured pressures and temperatures within the vessel and at the orifice on the CO₂ phase diagram. The rake of thermocouples in the experiments indicated that there was a degree of thermal stratification within the vessel, with temperatures varying by around 8 °C between the



Fig. 2. INERIS Test 8 showing the vapour cloud. The vertical column shown is at a distance of 10 m downstream from the orifice.

Table 1
Summary of experimental conditions.

	Test 2	Test 8
Average vessel pressure (barg)	26.8	60.9
Average vessel temperature (°C)	−9.6	5.9
Orifice diameter (mm)	6	25
Height of release (m)	1.5	1.5
Ambient temperature (°C)	−1.0	4.0
Ambient humidity (% RH)	90	95

highest and lowest sensors. The temperatures shown in Fig. 3 are taken from the thermocouple closest to the pipe connection in the vessel.

In Test 2, saturation conditions were present in the vessel and the points shown on the phase diagram (Fig. 3) lie on the liquid–vapour saturation curve. Unfortunately, the pressure transducer at the orifice failed in Test 2, but the dispersion results were consistent with the CO₂ being in a saturated liquid state in the pipe. In Test 8, a higher initial pressure of around 76 bar was used and the pressure and temperature measurements showed that liquid CO₂ was released through the orifice.

During the “steady” period of the release in Test 8, the pressure in the vessel fell from 76 bar to 55 bar and the temperature at the pipe inlet fell from 7 °C to 5 °C, over a 16 s period. Since the orifice diameter was much smaller in Test 2 (6 mm, instead of 25 mm in Test 8), the pressure and temperature change was less significant: a modest reduction from 28 bar to 27 bar and −10 °C to −9 °C, over a 100 s period.

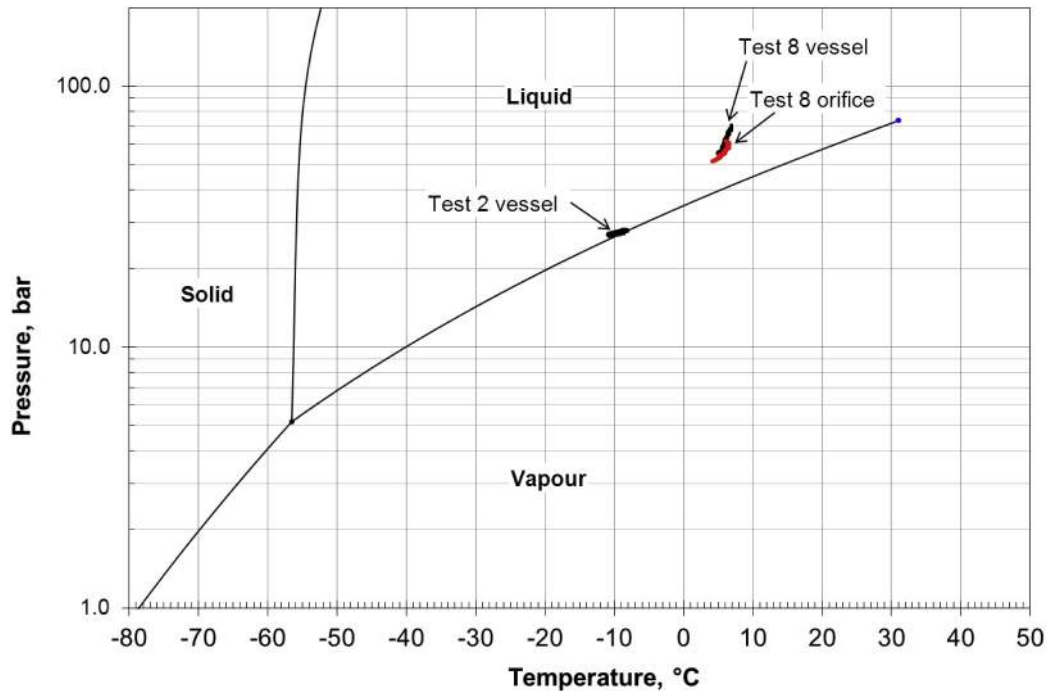


Fig. 3. Measured conditions inside the vessel and the orifice in INERIS Tests 2 and 8.

In order to specify the vessel conditions for the steady-state Phast calculations presented later, the averaged vessel pressures and temperatures shown in Table 1 have been used.

4. Dispersion models

4.1. DNV Phast

Phast is a hazard-assessment software package produced by DNV Software for modelling atmospheric releases of flammable or toxic chemicals (Witlox and Oke, 2008, Witlox, 2010). It includes methods for calculating discharge and dispersion, and toxic or flammable effects. A principal component of Phast is the Unified Dispersion Model (UDM), which incorporates sub-models for two-phase jets, heavy and passive dispersion, droplet rainout and pool spreading/evaporation. The model can simulate both unpressurised and pressurised releases, time-dependent releases (steady-state, finite-duration, instantaneous or time-varying), buoyancy effects (buoyant rising cloud, passive dispersion or heavy-gas-dispersion), complex thermodynamic behaviour (multiple-phase or reacting plumes), ground effects (soil or water, flat terrain with uniform surface roughness), and different atmospheric conditions (stable, neutral or unstable).

In the present work, Phast version 6.7 was used, which is described in the papers of Witlox et al. (2009, 2011, 2012). The guidance provided in the Phast version 6.6 release notes on the correct model configuration for CO₂ releases was followed. The discharge model based on conservation of mass, momentum and energy was used for the expansion from the orifice to ambient pressure (an option called “conservation of energy” in the Phast user interface). For the flow through the orifice, the Phast model was used that allows flashing to take place, rather than the default approach that assumes meta-stable liquid conditions, following the recommendations of Witlox et al. (2012). The use of this flashing model was found to have a significant effect on the results, including a reduction in the mass flow rate at the orifice of more

than 50% in Test 2, compared to the meta-stable liquid model prediction.

Phast cannot directly model the vessel, pipe and orifice plate configuration in the INERIS experiments. The “line-rupture” release model in Phast is only applicable for full-bore releases from short pipes, not releases through orifice plates at the end of short pipes. Since the frictional losses along the pipes in the INERIS tests were small compared to the losses through the orifice, simulations were performed using the Phast “vessel” model. The 6.3 m long length of pipe was therefore ignored and the orifice was instead assumed to be on the side of the vessel itself.

In the dispersing jet of CO₂, Phast’s UDM assumes that the two-phase flow is in homogeneous equilibrium. Both Witlox et al. (2012) and Dixon et al. (2012) have shown that this is a valid approximation for free-jet releases of dense-phase CO₂ through orifices of up to 2” (50.8 mm) diameter. Phast version 6.7 also assumes that the solid CO₂ particles remain within the dispersing jet and do not deposit on the ground. The previous work also demonstrated this to be a valid approximation in free, unimpeded jets.

4.2. ANSYS-CFX

The ANSYS-CFX dispersion model for two-phase CO₂ releases used a Lagrangian particle-tracking model to simulate the sublimating solid CO₂ particles in the jet. The process of sublimation was simulated using the standard droplet evaporation model in ANSYS-CFX version 14 (2011), with suitable Antoine equation coefficients for solid CO₂ sublimation. Drag between the CO₂ particles and surrounding gas phase was calculated using the drag model of Schiller and Naumann (1933) combined with the stochastic dispersion model of Gosman and Ioannides (1981) to account for turbulence effects. Heat transfer between the gas phase and solid particles was modelled using the Ranz–Marshall correlation (1952) and turbulence effects in the gas phase are modelled using the Shear-Stress Transport (SST) model of Menter (1994). These sub-

models are all available in the standard version of ANSYS-CFX version 14 (2011) and do not require user-coding.

To account for the effects of ambient humidity, the modelled gas phase consisted of a mixture of three components: dry air, CO₂ gas and water vapour. Each of these three phases was treated as an ideal gas. An additional dispersed-droplet Eulerian phase was used to account for condensed water droplets, which were assumed to have the same velocity as the surrounding gas phase. Source terms in the continuity and energy equations were used to model the process of water vapour condensation and evaporation. A similar approach was used previously by Brown and Fletcher (2003) to model atmospheric plumes from alumina refinery calciner stacks.

The computational grids used with ANSYS-CFX in the present work were unstructured, with tetrahedral cells clustered within the jet and prism-shaped cells along the ground (see Fig. 4). Previous tests (Dixon et al., 2012) showed that relatively fine grids are needed to resolve the sublimation process in two-phase CO₂ jets and therefore in excess of 0.6 million nodes were used in each of the ANSYS-CFX simulations presented here. Tests were performed using grids with roughly twice the number of nodes to confirm that the results were grid independent. A second-order accurate “high resolution” numerical method was used for the convective terms in both the momentum and turbulence model equations.

Source conditions for the CO₂ jet were prescribed in the ANSYS-CFX model at a location downstream from the orifice where the pressure had fallen to atmospheric pressure. Details of these source conditions are given in Section 4.4. Entrainment boundaries with no imposed wind speed were used on the domain boundaries upstream and downstream of jet. For the thermal boundary conditions, it was assumed that the stability of the atmospheric boundary layer was neutral (Pasquill “D” class). Previous work by Gant et al. (2013) has shown that dense-phase CO₂ jet dispersion behaviour is insensitive to the imposed wind conditions, due to the dominance of the jet momentum, for CO₂ concentrations down to 1% v/v (where the wind direction is co-flowing with the jet).

4.3. FLACS

The two-phase CO₂ dispersion model in the internal research and development version of FLACS (GexCon, 2011) also used a Lagrangian method for the solid CO₂ particles (Ichard, 2012). The governing equations solved for the continuous phase were the compressible form of the Reynolds-averaged Navier–Stokes (RANS) equations, where turbulence was modelled using a standard *k-ε* model (Lauder and Spalding, 1974; Hjertager, 1982). A two-way coupling between the continuous gas-phase and the dispersed particle-phase was established through source terms in the mass, momentum and energy equations (Peirano et al., 2006). In addition, particle–turbulence interaction was accounted for by source terms in the turbulent kinetic energy and dissipation rate equations (Mandø et al., 2009).

A simplified form of the Maxey & Riley’s (1983) original equation was used for the particle momentum equation, based on the analysis of Armenio and Fiorotto (2001). Both the buoyancy force and the drag force were included in the model, but the added-mass force and the Basset history force were ignored, since both are negligible when compared to the drag force (Armenio and Fiorotto, 2001). In addition, the pressure-gradient force term was also omitted, since its influence is small for large particle–fluid density ratios (Armenio and Fiorotto, 2001). The instantaneous fluid velocity seen by the particle, which is an unknown parameter in the particle momentum equation, was modelled through stochastic differential equations. A modified Langevin equation derived by Minier and Peirano (2001) was used for this purpose.

Droplet vaporization was modelled by an infinite liquid conductivity model (Aggarwal et al., 1984, 1995) with corrections to account for convective effects (Abramzon and Sirignano, 1989). Although it is not relevant for the present work, particle deposition and interaction with obstacles can be accounted for in the FLACS model (Crowe, 2006), but particle–particle interactions such as collisions, breakup and coalescence were not taken into account. In addition, humidity effects were not considered in the present version of the model.

The governing equations were solved on a staggered Cartesian grid (see Fig. 4) using a finite volume method. The solver for both the continuous and dispersed phases was second-order accurate. A central-differencing scheme was used for the diffusive fluxes, while a hybrid scheme with weighting between upwind and central-differences was used for the convective fluxes. Time-marching was carried out using an implicit backward-Euler scheme and the discretized equations were solved using a BICGStab iterative method with the SIMPLE pressure correction algorithm (Versteeg and Malalasekera, 2007). Further information concerning the FLACS Lagrangian particle-tracking model and its validation can be found in the PhD thesis of Ichard (2012).

The capabilities and limitations of FLACS for modelling vapour dispersion were reviewed previously by Gant and Hoyes (2010). This identified that one of the difficulties in using FLACS for modelling jets was the use of a Cartesian grid, where cells cannot easily be clustered together to refine the shear layers on the jet periphery. An overly coarse grid in these areas may lead to numerical diffusion, which tends to artificially increase the spreading rate of the jet. Another consequence of this grid arrangement is that high-aspect ratio cells are used in the far-field. To minimise the effects of numerical diffusion, in the present work each of the FLACS simulations used around 0.5 million grid cells.

4.4. CFD model source conditions

Both the ANSYS-CFX and FLACS models employed the same source conditions for the CO₂ jet that were taken from University of Leeds near-field model outputs (Woolley et al., 2013). These conditions consisted of radial profiles of velocity, temperature, CO₂

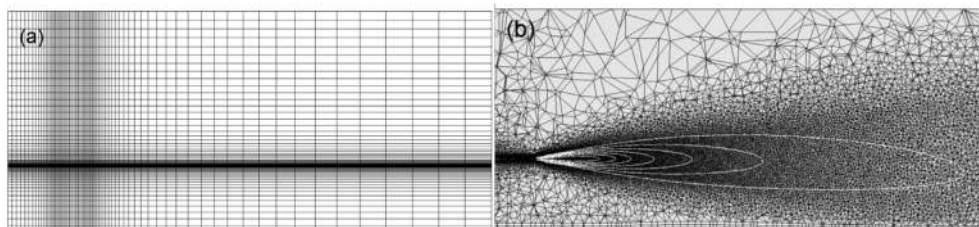


Fig. 4. Grid methodology in (a) FLACS: Cartesian structured mesh; (b) ANSYS-CFX: unstructured tetrahedral mesh.

solid and gas concentration, turbulent kinetic energy (k) and turbulence dissipation rate (ϵ), at a plane located at ten orifice diameters downstream from the actual orifice. This location was chosen since the jet has expanded to reach atmospheric pressure at this point.

The University of Leeds near-field dispersion model used inlet boundary conditions taken from pipe outflow model predictions produced by UCL, which consisted of the velocity, liquid mass fraction and temperature of the CO_2 at the orifice. Further details of the UCL modelling approach can be found in the paper by Brown et al. (2013).

Two different approaches were tested to interface the University of Leeds near-field model results and the far-field dispersion models. In the first approach (used with both ANSYS-CFX and FLACS), the axisymmetric radial profiles shown in Fig. 5 were used, where the velocity, temperature, CO_2 solid and gas concentration, k and ϵ varied across the radius of the jet. The same velocity field was

used for the gaseous and particulate phases. This approach was complex to implement and involved specifying more than a hundred separate annulus-shaped injection locations for the gaseous and particulate phases in ANSYS-CFX. In the FLACS model, a coarser resolution of the inlet profiles was used which involved 49 separate point leaks across the source area, with just five points across the jet radius. A large number of Lagrangian particles were needed with both codes. For the ANSYS-CFX model, 500 Lagrangian particles were injected at each annulus, giving rise to a total particle count of 86,000 in Test 2 and 56,000 in Test 8. Since FLACS used a transient solver, particles were injected continuously at each time-step until a steady solution was obtained. For Test 2, this meant that around 2.5 million particles were injected over the 4 s duration of the modelled release (125 particles per time-step) and 2.3 million particles in Test 8 over the 15 s release. One of the issues in running simulations on a standard desktop computer with such a high particle count is the computer memory requirements.

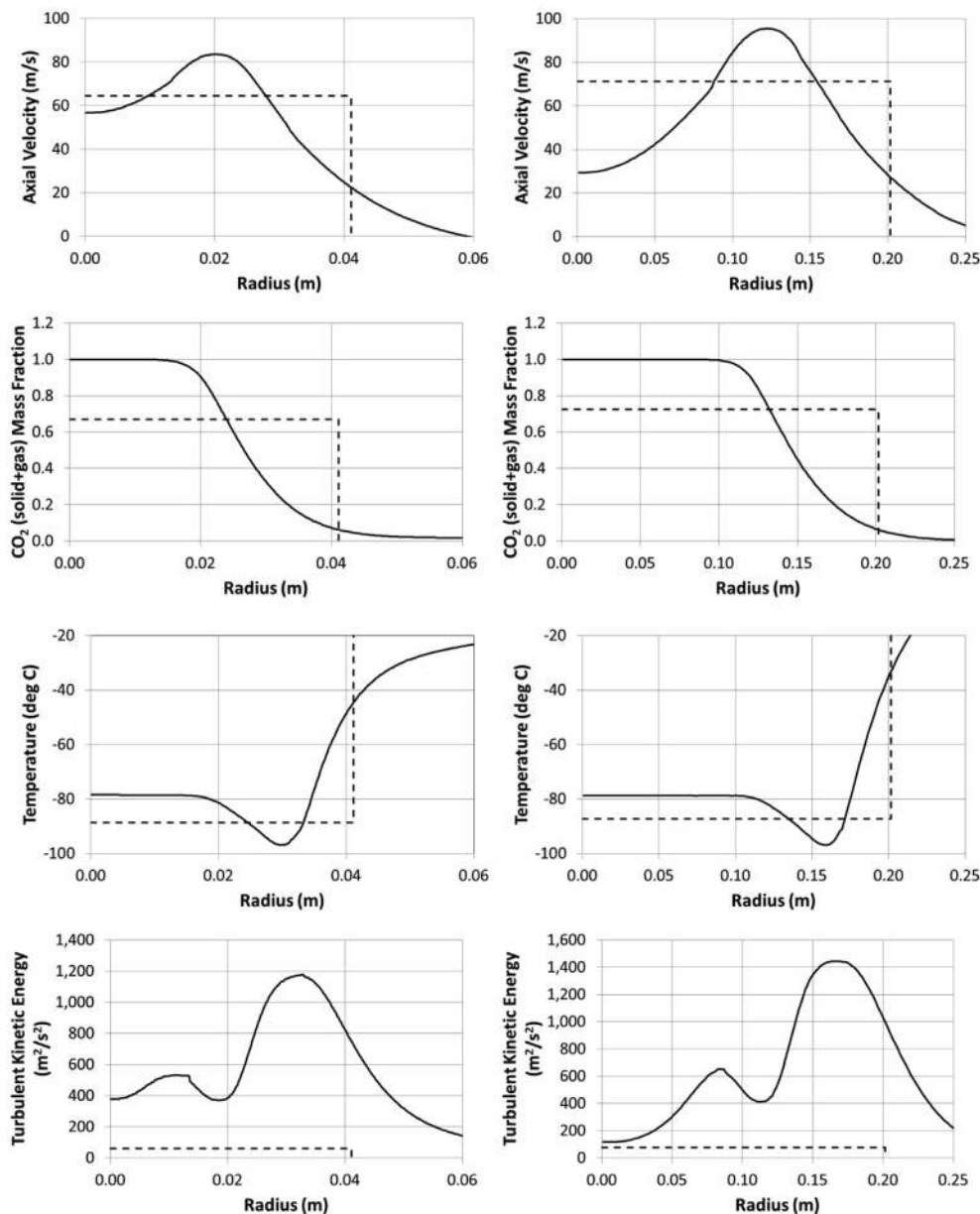


Fig. 5. Inlet profiles used by the CFD models for INERIS Tests 2 (left) and 8 (right): — University of Leeds near-field model results; - - : averaged (top hat) profiles.

The second approach for modelling the CO₂ source conditions (tested only with ANSYS-CFX) used the averaged (top-hat shaped) profiles shown in Fig. 5. These simpler source conditions were derived from the radial profiles by integrating across the source area whilst conserving mass, momentum and volume flux. The mean velocity was calculated from the ratio of the integrated momentum flux to the integrated mass flux, and the source area from the ratio of the integrated volume flux to the mean velocity. It was assumed that as the jet depressurizes, the conditions followed the liquid–vapour and then solid–vapour saturation curves in the pressure–temperature phase diagram (Fig. 3). The temperature was then determined from the averaged CO₂ partial pressure. For the turbulence conditions, k was specified assuming a turbulence intensity of 10%, and ϵ from assuming a turbulence length scale equal to 7% of the source diameter. These conditions are typical of the turbulence levels in jets (see, for example, Versteeg and Malalasekera, 2007). This approach of using 10% turbulence intensity and 7% diameter for the length scale was also used in the previous work of Dixon et al. (2012).

In the ANSYS-CFX model with the averaged source conditions, a total of 10,000 Lagrangian particles were injected at the source. This choice of particle count was based on previous work by Dixon et al. (2012) that showed it to be sufficient to produce results that were independent of the particle count.

The University of Leeds near-field model outputs did not include predictions of the CO₂ particle size, which is an important input for Lagrangian dispersion models. The size of the solid CO₂ particles produced by dense-phase CO₂ releases is uncertain, and it cannot be measured reliably in large-scale releases. Previous work has shown that dispersion models that assume homogeneous equilibrium provide reasonably good predictions of temperatures and concentrations in dense-phase CO₂ jets (Witlox et al., 2012; Dixon et al., 2012). Kukkonen et al. (1993) also showed that homogeneous equilibrium was a reasonable approximation for flashing jet releases of ammonia.

Homogeneous equilibrium models assume that the particles have the same temperature and velocity as the surrounding gas phase, which implies that the particles must be very small. Analysis of CO₂ particle sizes by Hulsbosch-Dam et al. (2012) suggested that the initial CO₂ particle diameter once the jet has expanded to atmospheric pressure should be in the range 1–20 μm .

In the ANSYS-CFX model, the CO₂ particles were assigned an initial uniform diameter of 20 μm at the inlet plane, and their diameter decreased downstream as the particles sublimated within the CO₂ jet, until they had reached a cut-off diameter of 0.01 μm , where they were assumed to have sublimated completely and were no longer tracked. A sensitivity test, using a smaller initial particle diameter of 5 μm , produced practically identical dispersion results.

In FLACS, the particle size was specified at the inlet plane in Test 2 using a log-normal distribution with a Sauter mean diameter of 7 μm , whilst in Test 8 a uniform particle diameter of either 10 μm or 20 μm was used. For the Test 8 simulations using 10 μm particles, numerical instability issues were encountered that meant that 4% of the mass of the solid CO₂ was not accounted for in the simulations.

5. Results

5.1. INERIS Test 2

The predicted temperature and concentration along the centreline of the jet for Test 2 are shown in Figs. 6 and 7. Model predictions are shown from Phast, ANSYS-CFX and FLACS, with two results shown from ANSYS-CFX, using either the radial inlet profiles from the University of Leeds model or the averaged top-hat shaped profiles (see Fig. 5). The experimental values are taken from averaging conditions over 100 s during the steady period of the release (which lasted around 130 s in total), when the temperatures and concentrations remained fairly constant (with the exception of the temperature at the mast nearest to the orifice – as discussed below).

All of the models predicted temperatures below the experimental measurements, with the exception of the measurement position nearest to the orifice (see Fig. 6). At the four positions further downstream, between 2 m and 5 m, the Phast results were around 10 °C lower than the measurements, whilst the FLACS and ANSYS-CFX temperatures were 20 °C to 30 °C lower. The higher temperatures in the case of Phast may be due to its discharge model predicting a lower mass release rate as compared to that used in the CFD models. Phast predicted a total (gas plus solid) CO₂ mass release rate of 0.54 kg/s, compared to 0.70 kg/s for the CFD models (from the UCL outflow model, see Brown et al., 2013). The measured release rate was 0.78 kg/s \pm 0.2 kg/s.

The sharp change in the slope of the Phast temperature curve in Fig. 6 was due to the model's treatment of the sublimating CO₂ particles. From the orifice up to a distance of around 1.1 m, the model predicted progressively lower temperatures as air was entrained into the jet and the CO₂ particles sublimated. The temperature followed the saturation curve in the phase diagram (Fig. 3) as the partial pressure of CO₂ decreased. At a distance of around 1.1 m, all of the particles had sublimated and further downstream from there, as air was entrained into the gaseous CO₂ jet it caused the temperature to rise until eventually it reached the ambient temperature.

All of the models predicted higher temperatures than were measured at the first mast. The measurement here was probably

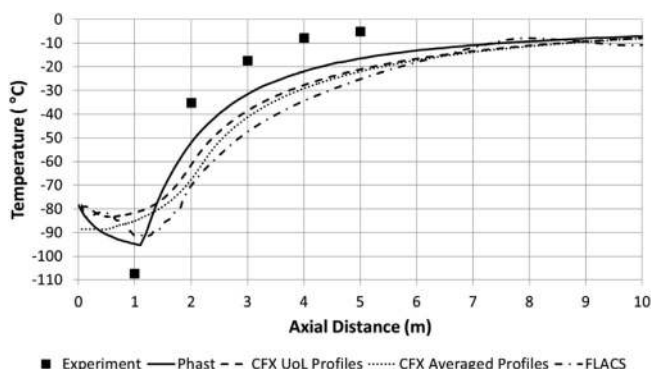


Fig. 6. Temperature along the centreline of the jet in INERIS Test 2.

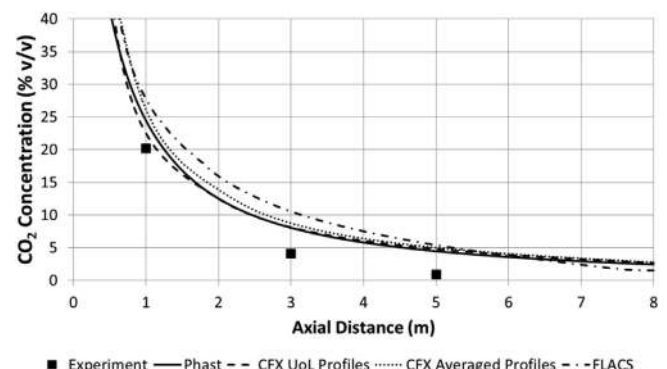


Fig. 7. CO₂ gas concentration along the centreline of the jet in INERIS Test 2.

unreliable since at times it recorded temperatures as low as $-180\text{ }^{\circ}\text{C}$. It is difficult therefore to draw any conclusions from this particular result, except to conclude that both models and measurements obtained temperatures close to the orifice that were lower than the sublimation temperature at atmospheric pressure of $-78\text{ }^{\circ}\text{C}$.

The FLACS predictions differed from ANSYS-CFX, despite both models using the same inlet profiles and both models being based on the same underlying principle of Lagrangian particle tracking. In the near-field, the FLACS temperatures reached a minimum temperature of $-92\text{ }^{\circ}\text{C}$, compared to $-83\text{ }^{\circ}\text{C}$ with ANSYS-CFX. One possible explanation for this behaviour is the smaller CO_2 particle size in the FLACS model, which used a Sauter mean diameter of $7\text{ }\mu\text{m}$. However, tests conducted with ANSYS-CFX showed that it produced practically identical results using an initial particle diameter of $5\text{ }\mu\text{m}$ instead of $20\text{ }\mu\text{m}$. Another potential reason for the lower temperature with FLACS is the use of a Cartesian grid which may have under-resolved the shear layers on the edge of the expanding jet. This could have led to numerical diffusion effects, which would artificially increase the jet spreading rate, leading to higher entrainment rates and lower temperatures. However, a relatively fine grid of around 0.5 million cells was used in the FLACS simulations, so these effects should be small. A more likely explanation is the resolution of the source profiles. FLACS used just 5 points across the source radius, whereas ANSYS-CFX used around 47 cells and 172 separate particle injection locations across the source radius to resolve the profiles shown in Fig. 5.

Further downstream in the jet, at around 8 m from the orifice, the FLACS temperature started to fall from a maximum of $-8\text{ }^{\circ}\text{C}$, rather than continue to rise to the ambient temperature of $-1\text{ }^{\circ}\text{C}$. The cause of this behaviour may relate to the proximity of the CFD domain outflow boundary, the use of zero wind speed conditions or the transient simulation process.

The temperature at the inlet plane was $-89\text{ }^{\circ}\text{C}$ with the version of the ANSYS-CFX model that used the averaged University of Leeds profiles. This low temperature was due to the way in which the averaged source conditions were calculated. The inlet plane was located at a distance of ten orifice diameters downstream from the orifice and the near-field model predictions from the University of Leeds showed that some air was entrained into the jet within this

near-field region. The resulting average CO_2 vapour pressure was 56 kPa and, in order to maintain solid-vapour equilibrium, this implied an average temperature of $-89\text{ }^{\circ}\text{C}$.

The Phast predictions of concentration (Fig. 7) were generally within 1% v/v of the ANSYS-CFX values. Close to the orifice, however, the ANSYS-CFX model using the averaged source conditions predicted concentrations that were around 2% v/v higher than Phast's. Both the Phast and ANSYS-CFX model predictions were around 3–5% v/v higher than the measured values at the three measurement positions. This difference is significant, as it is comparable to the Immediately Dangerous to Life and Health (IDLH) concentration for CO_2 of 4% v/v (NIOSH, 1995). From a hazard-assessment perspective, the models predicted conservative concentrations and if the maximum extent of the hazardous cloud is taken to be where the concentration is equal to the IDLH value, the models predict the hazard range to extend approximately twice as far as was measured (6 m as compared to 3 m).

FLACS predicted concentrations that were up to 2% v/v higher than Phast and ANSYS-CFX in the region between 1 m and 4 m from the orifice. However, at a distance of 5 m, where the concentrations approached the IDLH value, the model predictions were all in close agreement with each other (within 1% v/v).

In terms of the source term treatment in the ANSYS-CFX model, the use of averaged rather than complex radial profiles had a relatively modest effect in Test 2. Fig. 8 shows the predicted temperature field using the two different source conditions and the two results here appear similar in terms of the spreading rate of the jet and the shape of the temperature contours.

5.2. INERIS Test 8

In Test 8, temperature measurements were made at the four masts nearest the orifice using five thermocouples on each mast, which were arranged vertically through the jet. In the 16 s release period, measurements on the two masts nearest the orifice indicated that the jet width changed over time. To illustrate this, the temperatures from the mast at 2 m are shown in Fig. 9. In the first 5 s of the release, the CO_2 jet was wide and the thermocouples 0.4 m above and below the centreline registered temperatures of around $-65\text{ }^{\circ}\text{C}$. Shortly thereafter, the jet narrowed and the same thermocouples registered temperatures of only around $-5\text{ }^{\circ}\text{C}$ in the period between 10 s and 15 s. The initial behaviour in the first 5 s is thought to result from pressure transients produced by opening the valves and the establishment of the jet. The mean temperatures shown in the subsequent plots (Figs. 10 and 12) have therefore been produced by averaging the later “steady” period of the release between 10 s and 15 s. Solid square symbols are used for the mean

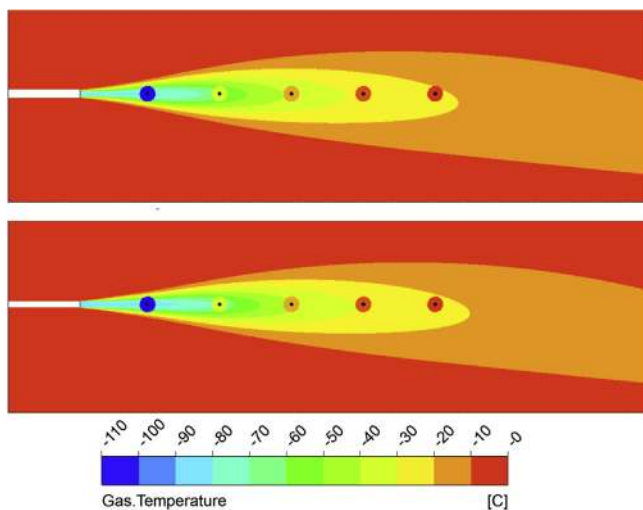


Fig. 8. Contours of predicted temperature for INERIS Test 2 using ANSYS-CFX with the full University of Leeds inlet profiles (top) and averaged inlet profiles (bottom). Coloured circles show the experimental values. (For interpretation of the references to colour in this figure legend, the reader is referred to the web version of this article.)

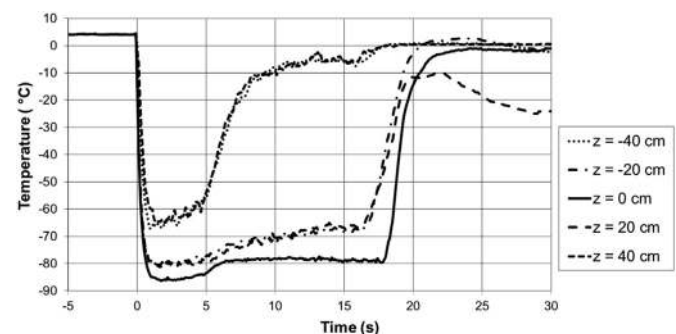


Fig. 9. Temperatures recorded in INERIS Test 8 on Mast 2 at five different vertical locations 0.2 m apart, from 0.4 m below the jet centreline to 0.4 m above.

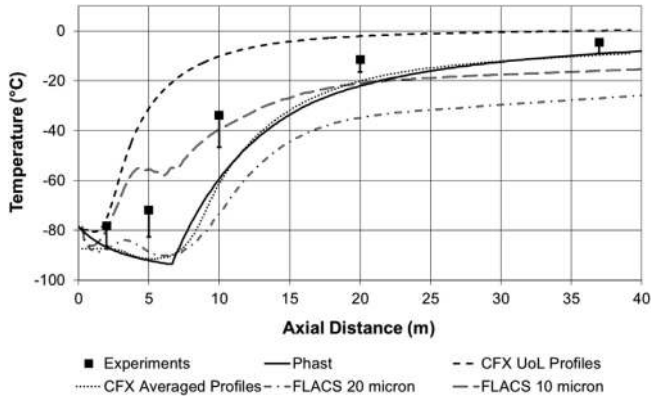


Fig. 10. Temperature along the centreline of the jet in INERIS Test 8.

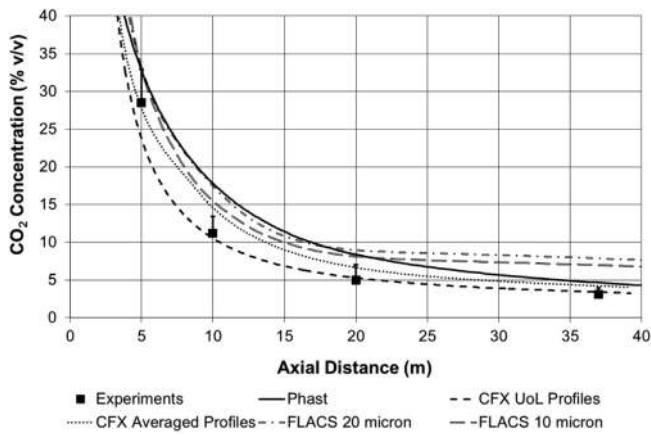


Fig. 11. CO₂ gas concentration along the centreline of the jet in INERIS Test 8.

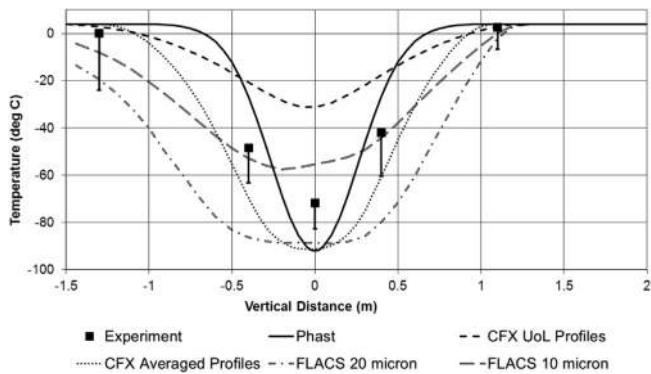


Fig. 12. Vertical profiles of temperature 5 m downstream from the orifice for INERIS Test 8.

temperature and an error bar is used to show the minimum temperature recorded during the earlier part of the release.

Regarding the oxygen cell measurements, the first two masts nearest the orifice produced unreliable measurements due to the low temperatures and high velocity flow. At the remaining masts, the concentrations showed a similar trend to the temperatures, with slightly higher initial CO₂ concentrations decreasing over time to reach a lower plateau. The mean concentrations shown in the model comparisons (Fig. 11) are the averaged values during the

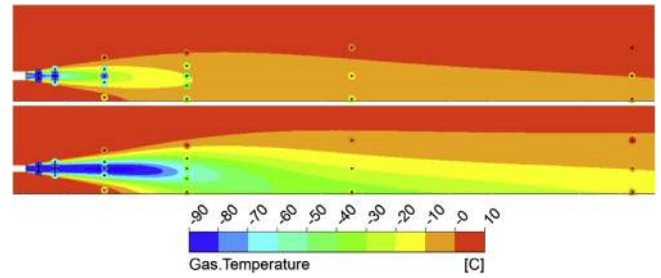


Fig. 13. Contours of predicted temperature for INERIS Test 8 using ANSYS-CFX with the full University of Leeds inlet profiles (top) and averaged inlet profiles (bottom). Coloured circles show the experimental values on the masts located at 1 m, 2 m, 5 m, 10 m, 20 m and 37 m from the orifice. (For interpretation of the references to colour in this figure legend, the reader is referred to the web version of this article.)

later, steady period of the release, and an error bar is used to show the maximum concentration recorded at earlier times.

The predicted temperatures and concentrations along the centreline of the jet are compared to the measurements in Figs. 10 and 11. The models produced a wide range of predicted temperatures. For example, at 10 m downstream from the orifice, the FLACS model with 20 μm particles predicted a temperature of −73 °C whereas the ANSYS-CFX model with the full radial jet inlet profiles predicted a temperature of only −10 °C. The differences are less significant in terms of CO₂ concentration, but the disparity between minimum and maximum predictions is still around 8% v/v (i.e. twice the IDLH). The FLACS model using the same inlet profiles and particle size as the ANSYS-CFX model consistently produced between 3 and 7% vol/vol higher concentrations.

The Phast model and the ANSYS-CFX model using the averaged source conditions produced predictions in close agreement with each other, but consistently under-predicted the temperatures by up to 20 °C and over-predicted the concentrations by up to 8% v/v. The ANSYS-CFX predictions with the University of Leeds inlet profiles show the best agreement with the mean concentrations of all the different models, but still over-predicted the temperatures by up to 35 °C at all but the first measurement position.

The fact that the ANSYS-CFX model is sensitive to the choice of inlet boundary conditions is at odds with the behaviour observed in the previous Test 2 results. To investigate whether it resulted from the inlet turbulence levels, a simulation was performed using the University of Leeds inlet profiles for all parameters except *k* and *ε*, for which the averaged top-hat shaped profiles were used. The results from this test are not shown, but they did not exhibit a significant change in behaviour from the results using the full radial profiles for *k* and *ε*, so it seems unlikely that the initial turbulence levels were responsible for producing overly high levels of entrainment.

The reason for the differences in model behaviour using the two inlet profiles appears to have been related to the behaviour of the solid CO₂ particles, which sublimated more slowly with the averaged source conditions (Fig. 14). Using the averaged source conditions, the particles released across the source were in equilibrium with the surrounding vapour. The source temperature and CO₂ vapour concentration was such that particles could not sublime until air had been entrained into the jet. In contrast, with the University of Leeds radial inlet profiles, the concentration and temperature varied across the width of the jet and released particles (whose trajectory was perturbed by turbulent dispersion) soon encountered regions of the flow where they could rapidly sublime.

The FLACS predictions showed a significant sensitivity to the size of the solid CO₂ particles. Using an initial particle diameter of

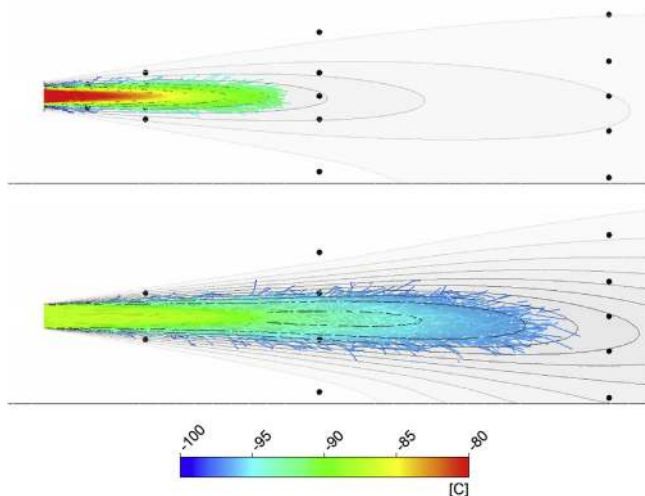


Fig. 14. Solid CO₂ particle trajectories coloured according to the particle temperature in INERIS Test 8 using ANSYS-CFX with the full University of Leeds inlet profiles (top) and averaged inlet profiles (bottom). Black symbols show the location for the thermocouples used in the experiments, located at 2 m, 5 m and 10 m from the orifice.

20 μm produced temperatures around 35 °C lower than those predicted using 10 μm particles at a distance of 10 m. These differences persisted into the far-field and even at 40 m downstream, there were still differences of around 12 °C. This behaviour was not observed with the ANSYS-CFX model, which produced practically identical results using either 20 μm or 5 μm particles. Such a high sensitivity to the particle size is in contrast to the previous trends observed by Hill et al. (2011) and Kukkonen et al. (1993). One possible explanation is that the numerical instability problems that were encountered in the simulations with 10 μm particles, which meant that 4% of the solid CO₂ mass was not accounted for by the model, produced a significant effect on the temperatures and concentrations.

Fig. 12 shows that the differences between the two FLACS results persisted across the width of the jet. The graph also shows that both the 10 μm and 20 μm FLACS models predicted the jet to spread more rapidly than the ANSYS-CFX and Phast predictions. The jet therefore reached the ground sooner, which led to a reduction in the air entrainment rate into the jet. This may explain the concentration behaviour shown in Fig. 11, where the slope of the two FLACS curves decreases at a distance of around 20 m, due to the reduced entrainment.

5.3. Discussion

The performance of the dispersion models presented above for the INERIS Tests 2 and 8 (Figs. 6–14) is generally poorer than that observed previously in other dense-phase CO₂ jet validation studies by Witlox et al. (2012) and Dixon et al. (2012). In the Dixon et al. (2012) study, the ANSYS-CFX model predictions were mostly within 1–2 % vol/vol of the CO₂ concentration measurements, and within 5 °C of the measured temperatures. Despite using the same model, in the present work these differences were between 3 and 5% vol/vol in CO₂ concentration and 5–35 °C in temperature.

There are two main differences between the Dixon et al. (2012) work and the present study. Firstly, the way in which the jet inlet boundary conditions in the ANSYS-CFX model were specified was different. In the Dixon et al. (2012) work, the boundary conditions were specified using averaged (top-hat shaped) profiles produced by an integral model for outflow and jet expansion (the Shell FRED model, Betteridge and Roy, 2010), instead of the near-field model of

University of Leeds (Woolley et al., 2013). The FRED model makes a number of assumptions concerning conservation of mass, momentum and energy, and assumes homogeneous equilibrium between the two phases, whilst the University of Leeds model solves the axisymmetric, compressible Reynolds-averaged Navier–Stokes equations and allows for a degree of phase slip. Although this choice of inlet boundary conditions clearly has an effect (as demonstrated by the marked difference in results when the University of Leeds source profiles were averaged), this probably does not explain all of the differences.

The second potential reason for the differences relates to the experimental arrangements. In the Shell experiments studied by Dixon et al. (2012), the liquid CO₂ was contained in a 24" diameter vessel with a volume of 6.3 m³, which was connected at one end to an inclined pipe filled with liquid CO₂ at the same conditions as within the vessel. The inlet to this inclined pipe was then connected to a nitrogen reservoir at a constant supply pressure, in order to produce a steady discharge from the orifice. Pressures upstream of the orifice were maintained at around 145 barg and 127 barg in the two free-jet releases examined by Dixon et al. (2012) (Shell Tests 3 and 5), which used orifice diameters of ½" (12.7 mm) and 1" (25.4 mm), respectively. In contrast, in the INERIS experiments, a smaller, isolated 2 m³ vessel was used to contain the liquid CO₂ and in Test 8 the pressure fell from 76 bar to 55 bar over the 16 s release period.

As the vessel pressure falls, the velocity of the CO₂ jet would decrease and therefore the rate of air entrainment into the jet should also decrease. These effects can balance each other out and result in the concentrations far downstream in the jet remaining relatively unaffected (Gant et al., 2013). However, closer to the orifice, in the region where the measurements were undertaken, the change in CO₂ mass flow rate and the proportion of solid CO₂ over time may have affected the temperature and concentration measurements.

Another difference between the Shell and INERIS experiments relates to the interpretation of the measurement data. In the Shell experiments, the oxygen cells were found to have been adversely affected by low temperatures in the jet, and therefore the concentrations used in the model validation study were taken from measurements in the early period of the release, when the oxygen concentration was at its minimum (corresponding to the peak CO₂ concentration). This matter was discussed by both Witlox et al. (2012) and Dixon et al. (2012). In the INERIS tests, however, the peak in CO₂ concentrations was considered to result from initial transient behaviour (before the jet had become fully established) and the mean concentrations at a later time were used instead. To provide an indication of the difference between the peak and mean values in the INERIS tests, the peak concentrations are shown using error bars in Fig. 11. Depending upon whether the peak or the mean is taken as the true experimental value, the agreement with various models is different.

To investigate this matter further and provide more precise comparisons of models and measurements, one option would be to perform transient simulations of INERIS Test 8, in order to resolve the time-varying behaviour. However, given the computing time and difficulty in interfacing near-field and far-field models, this approach has not yet been pursued.

6. Conclusions

Dispersion model predictions from Phast, FLACS and ANSYS-CFX have been compared to measurements from two dense-phase CO₂ jet release experiments conducted by INERIS, as part of the EU-funded CO₂PipeHaz project. The first experiment involved a saturated liquid CO₂ release through a 6 mm orifice and the second a

pressurized liquid release from an initial pressure of 76 bar through a 25 mm orifice. In both cases, the FLACS and ANSYS-CFX models used inlet boundary conditions for the expanded CO₂ jet that were taken from a sophisticated near-field CFD model produced by the University of Leeds. Two different ways of interfacing this near-field model to the ANSYS-CFX far-field dispersion model were tested.

Overall, the predicted concentrations from the various models were in reasonable agreement with the measurements, but generally in poorer agreement than has been reported previously for similar dispersion models in other dense-phase CO₂ release experiments. In the first experiment (INERIS Test 2), all of the models consistently over-predicted the CO₂ concentrations by between 3 and 7% vol/vol. As a result, the distance from the orifice to the point where the CO₂ concentration fell to the IDLH value of 4% vol/vol was over-predicted by a factor of two.

In the second experiment with a larger orifice, a wide range of predictions were obtained using the different models. The ANSYS-CFX model was sensitive to the way in which the source conditions were specified (using either radial profiles from the University of Leeds model or averaged, top-hat shaped profiles). The FLACS model also showed significant sensitivity to the initial solid CO₂ particle size, producing different results with 10 µm or 20 µm particles, whereas the ANSYS-CFX model showed no sensitivity to the particle size within this range. Comparing the two model predictions to each other, FLACS consistently predicted concentrations of between 3 and 7% vol/vol higher than ANSYS-CFX, despite both models using the same inlet profiles and particle size, and both being based on Lagrangian particle tracking. The cause of this may be related to differences in the resolution of the CO₂ jet source and the computational grid, but further work is needed to investigate this. Phast produced similar results to the ANSYS-CFX model that used averaged top-hat inlet profiles, i.e. it consistently under-predicted the centreline temperatures by up to 20 °C and over-predicted the centreline concentrations by up to 8% v/v.

Whilst the ANSYS-CFX model with the radial jet inlet profiles from the University of Leeds model produced the best predictions of concentration in the second test, it produced fairly poor temperature predictions. The difficulties in interpreting these results were discussed, and it was noted that the experiments exhibited some time-varying behaviour, perhaps related to the pressure falling from 76 bar to 55 bar over the 16 s release period. The dispersion models, on the other hand, assumed jet inlet boundary conditions that remained unchanged over time.

One of the objectives of the present study was to investigate whether far-field CO₂ dispersion model predictions could be improved by using inlet profiles from the University of Leeds model that simulates the complex multi-phase, compressible jet behaviour close to the release point. Due to the inconsistencies in different far-field model predictions and difficulties in interpreting the measurements (particularly in the second test), further work is needed before definitive conclusions can be made on the merits of this approach. This should include a more thorough investigation of the causes of the differences between FLACS and ANSYS-CFX and examination of other experiments. Whilst the present work has focused on free-jet releases of dense-phase CO₂, more complex scenarios should also be examined in the future, such as releases from buried pipelines and impinging jets in congested and/or confined spaces.

Acknowledgements

The authors are grateful to the European Commission for funding this work under the 7th Framework Energy Program (Project Reference: 241346). The contribution made to this paper by Simon Gant (HSL) was also part-funded by the Health and Safety

Executive (HSE). The contents, including any opinions and/or conclusions expressed, are those of the authors alone and do not necessarily reflect HSE policy. The authors would like to thank the other participants of the CO₂PipeHaz project who contributed to this work. In particular, the project coordinators at UCL (Professor Haroun Mahgerefteh and Dr. Sergey Martynov), and the University of Leeds partners (Dr. Robert Woolley, Professor Mike Fairweather and Professor Sam Falle).

References

- Abramzon, B., Sirignano, W.A., 1989. Droplet vaporization model for spray combustion calculations. *Int. J. Heat Mass Transf.* 32, 1605–1618.
- Aggarwal, S.K., Sirignano, W.A., Tong, A.Y., 1984. A comparison of vaporization models in spray calculations. *AIAA J.* 22, 1448–1457.
- Aggarwal, S.K., Peng, F., 1995. A review of droplet dynamics and vaporization modeling for engineering calculations. *J. Eng. Gas Turbines Power* 117, 453–461.
- Ahmad, M., Buit, L., Florisson, O., Hulsbosch-Dam, C., Bögemann-van Osch, M., Spruijt, M., Davolio, F., 2013a. Experimental investigation of CO₂ outflow from a high-pressure reservoir. *Energy Proced.* 37, 3005–3017.
- Ahmad, M., Bögemann-van Osch, M., Buit, L., Florisson, O., Hulsbosch-Dam, C., Spruijt, M., Davolio, F., 2013b. Study of the thermohydraulics of CO₂ discharge from a high pressure reservoir. *Int. J. Greenh. Gas Control* 19, 63–73.
- ANSYS, 2011. ANSYS-CFX-solver Theory Guide. Release 14.0, November 2011.
- Armenio, V., Fiorotto, V., 2001. The importance of the forces acting on particles in turbulent flows. *Phys. Fluids* 13, 2437–2440.
- Betteridge, S., Roy, S., 2010. Shell FRED Technical Guide. Issue 6.0.
- Brown, G.J., Fletcher, D.F., 2003. CFD prediction of odour dispersion and plume visibility for alumina refinery calciner stacks. In: 3rd Int. Conf. on CFD in the Minerals and Process Industries. CSIRO, Melbourne, Australia, 10–12 December 2003.
- Brown, S., Martynov, S., Mahgerefteh, H., Proust, C., 2013. A homogeneous relaxation flow model for the full bore rupture of dense phase CO₂ pipelines. *Int. J. Greenh. Gas Control* 17, 349–356.
- Cleaver, P., Halford, A., Warhurst, K., 2013. Crater size and its influence on releases of CO₂ from buried pipelines. In: 4th International Forum on Transportation of CO₂ by Pipeline. Tiratsoo Technical, Clarion Technical Conferences, Gateshead, UK, 19–20 June 2013.
- Cooper, R., 2012. National Grid's COOLTRANS research programme. *J. Pipeline Eng.* 11, 155–172.
- Crowe, C., 2006. Multiphase Flow Handbook. In: Mechanical Engineering Series. CRC. ISBN 9780849312809.
- Dixon, C.M., Hasson, M., 2007. Calculating the release and dispersion of gaseous, liquid and supercritical CO₂. In: IMechE Seminar on Pressure Release, Fires and Explosions, London, 2 October 2007.
- Dixon, C.M., Heynes, O., Hasson, M., 2009. Assessing the hazards associated with release and dispersion of liquid carbon dioxide on offshore platforms. In: Paper 1651, 8th World Congress of Chemical Engineering, Montreal, 23–27 August 2009.
- Dixon, C.M., Gant, S.E., Obiorah, C., Bilio, M., 2012. Validation of dispersion models for high pressure carbon dioxide releases. In: IChemE Hazards XXIII Conference, Southport, UK, 12–15 November 2012.
- Gant, S.E., 2012. Framework for validation of pipeline release and dispersion models for the COOLTRANS project. In: 3rd International Forum on the Transportation of CO₂ by Pipeline, Newcastle, UK, 20–21 June 2012.
- Gant, S.E., Hoyes, J., 2010. Review of FLACS Version 9.0: Dispersion Modelling Capabilities. Health and Safety Executive (HSE) Research Report RR779. <http://www.hse.gov.uk/research/rrhtm/rr779.htm> (accessed 28.01.14.).
- Gant, S.E., Kelsey, A., 2012. Accounting for the effect of concentration fluctuations for gaseous releases of carbon dioxide. *J. Loss Prev. Process Ind.* 25, 52–59.
- Gant, S.E., Kelsey, A., McNally, K., Witlox, H.W.M., Bilio, M., 2013. Methodology for global sensitivity analysis of consequence models. *J. Loss Prev. Process Ind.* 26, 792–802.
- GexCon, 2011. FLACS v9.1 User's Manual, 2011. <http://www.flacs.com> (accessed 28.01.14.).
- Gosman, A.D., Ioannides, E., 1981. Aspects of Computer Simulation of Liquid Fuelled Combustors. American Institute of Aeronautics and Astronautics. AIAA Paper 81-0323.
- Harper, P., 2011. Assessment of the Major Hazard Potential of Carbon Dioxide (CO₂). Health and Safety Executive (HSE). <http://www.hse.gov.uk/carboncapture/assets/docs/major-hazard-potential-carbon-dioxide.pdf> (accessed 28.01.14.).
- Hill, T.A., Fackrell, J.E., Dubal, M.R., Stiff, S.M., 2011. Understanding the consequences of CO₂ leakage downstream of the capture plant. *Energy Proced.* 4, 2230–2237 (also published in: Int. Conf. On Greenhouse Gas Technologies, GHGT-10, September 2010).
- Hjertager, B.H., 1982. Simulation of transient compressible turbulent reactive flows. *Combust. Sci. Technol.* 27, 159–170.
- Hulsbosch-Dam, C.E.C., Spruijt, M.P.N., Trijssenaar-Buhre, I.J.M., 2011. Computational fluid dynamics study on two-phase CO₂ dispersion in a neutral atmosphere. In: 14th Conference on Harmonisation within Atmospheric Dispersion Modelling for Regulatory Purposes, Kos, Greece, 2–6 October 2011.

- Hulsbosch-Dam, C.E.C., Spruijt, M.P.N., Necci, A., Cozzani, V., 2012. Assessment of particle size distribution in CO₂ accidental releases. *J. Loss Prev. Process Ind.* 25, 254–262.
- Ichard, M., 2012. Numerical Computations of Pressurized Liquefied Gas Releases into the Atmosphere (PhD thesis). University of Bergen, Bergen, Norway. ISBN: 978-82-308-2010-0.
- Jamois, D., Proust, C., Hebrard, J., Gentilhomme, O., 2013. La sécurité du captage et du stockage du CO₂: un défi pour les industries de l'énergie. In: *XIV^e Congrès de la Société Française de Génie des Procédés (SFGP)*, Lyon, France, 8–10 October 2013. Récents Progrès en Génie des Procédés, Numéro 104 – 2013, ISSN: 1775-335X ; ISBN: 978-2-910239-78-7. SFGP, Paris, France, 2013.
- Kukkonen, J., Kulmala, M., Nikmo, J., Vesala, T., Webber, D.M., Wren, T., 1993. Aerosol Cloud Dispersion and the Suitability of the Homogeneous Equilibrium Approximation. AEA/Health and Safety Executive Working Paper HSE/CS/231/WP2, 18 August 1993.
- Launer, B.E., Spalding, D.B., 1974. The numerical computation of turbulent flows. *Comput. Methods Appl. Mech. Eng.* 3, 269–289.
- Mack, A., Spruijt, M.P.N., 2013a. Validation of OpenFOAM for heavy gas dispersion applications. *J. Hazard. Mater.* 262, 504–516.
- Mack, A., Spruijt, M.P.N., 2013b. CFD investigation of CO₂ worst case scenarios including terrain and release effects. In: 7th Trondheim CCS Conf., TCCS-7, Trondheim Norway, 5–6 June 2013.
- Mahgerefteh, H., Brown, S., Martynov, S., 2012. A study of the effects of friction, heat transfer, and stream impurities on the decompression behaviour in CO₂ pipelines. *Greenh. Gases Sci. Technol.* 2, 369–379.
- Mandø, M., Lightstone, M., Rosendahl, L., Yin, C., Sørensen, H., 2009. Turbulence modulation in dilute particle-laden flow. *Int. J. Heat Fluid Flow* 30, 331–338.
- Maxey, M.R., Riley, J.J., 1983. Equation of motion for a small rigid sphere in a nonuniform flow. *Phys. Fluids* 26, 883–889.
- Mazzoldi, A., Hill, T., Colls, J.J., 2008a. CFD and Gaussian atmospheric dispersion models: a comparison for leak from carbon dioxide transportation and storage facilities. *Atmos. Environ.* 42, 8046–8054.
- Mazzoldi, A., Hill, T., Colls, J.J., 2008b. CO₂ transportation for carbon Capture and Storage: sublimation of carbon dioxide from a dry ice bank. *Int. J. Greenh. Gas Control* 2, 210–218.
- Mazzoldi, A., Hill, T., Colls, J.J., 2011. Assessing the risk for CO₂ transportation within CCS projects, CFD modelling. *Int. J. Greenh. Gas Control* 5, 816–825.
- Menter, F.R., 1994. Two-equation eddy-viscosity turbulence models for engineering applications. *AIAA J.* 32, 1598–1605.
- Minier, J.-P., Peirano, E., 2001. The pdf approach to turbulent polydispersed two-phase flows. *Phys. Reports* 352, 1–214.
- Nielsen, M., Ott, S., 1995. A Collection of Data from Dense Gas Experiments. Risø Laboratory Report: Risø-R-845(En), ISBN 87-550-2113-1. http://www.risoecampus.dtu.dk/Research/sustainable_energy/energy_systems/projects/REDIPHEM.aspx?sc_lang=en (accessed 28.01.14.).
- NIOSH, 1995. Documentation for Immediately Dangerous to Life or Health Concentrations (IDLH). National Institute for Occupational Safety and Health (NIOSH) chemical listing and documentation of revised IDLH values (as of 3/1/95), NTIS publication no. PB-94-195047.
- Peirano, E., Chibbaro, S., Pozorski, J., Minier, J.-P., 2006. Mean-field/PDF numerical approach for polydispersed turbulent two-phase flows. *Prog. Energy Combust. Sci.* 32, 315–371.
- Perry, R.H., 2007. In: Green, D.W. (Ed.), *Perry's Chemical Engineer's Handbook*, eighth ed. McGraw-Hill, New York, USA. ISBN 978-0-07-142294-9.
- Pursell, M., 2012. Experimental investigation of high pressure liquid CO₂ release behaviour. In: Proc. IChemE Hazards XXIII Conference, Southport, UK, 12–15 November 2012.
- Ranz, W.E., Marshall, W.R., 1952. Evaporation from drops. *Chem. Eng. Prog.* 48, 141–173.
- Schiller, L., Naumann, A., 1933. Über die grundlegenden berechnungen bei der schwerkraftaufbereitung. *Ver. Dtsch. Ing.* 77, 318–320.
- Versteeg, H.K., Malalasekera, W., 2007. *An Introduction to Computational Fluid Dynamics: the Finite Volume Method*, second ed. Pearson Education Ltd.
- Wareing, C.J., Woolley, R.M., Fairweather, M., Falle, S.A.E.G., Cleaver, R.P., 2013. Large-scale validation of a numerical model of accidental releases from buried CO₂ pipelines. *Comput. Aided Chem. Eng.* 32, 229–234.
- Webber, D.M., 2011. Generalising two-phase homogeneous equilibrium pipeline and jet models to the case of carbon dioxide. *J. Loss Prev. Process Ind.* 24, 356–360.
- Wen, J., Heidari, A., Xu, B., Jie, H., 2013. Dispersion of carbon dioxide from vertical vent and horizontal releases – a numerical study. *Proc. Inst. Mech. Eng. E: J. Process Mech. Eng.* 227, 125–139.
- Witlox, H.W.M., 2010. Overview of consequence modelling in the hazard assessment package Phast. In: 6th AMS Conference on Applications of Air Pollution Meteorology, Atlanta, USA, 17–21 January 2010.
- Witlox, H.W.M., Harper, M., Oke, A., 2009. Modelling of discharge and atmospheric dispersion for carbon dioxide releases. *J. Loss Prev. Process Ind.* 22, 795–802.
- Witlox, H.W.M., Oke, A., 2008. Verification and validation of consequence models for accidental releases of hazardous chemicals to the atmosphere. In: Proc. IChemE Hazards XX Symposium & Workshop, Manchester, UK, 15–17 April 2008.
- Witlox, H.W.M., Stene, J., Harper, M., Nilsen, S.H., 2011. Modelling of discharge and atmospheric dispersion for carbon dioxide releases including sensitivity analysis for wide range of scenarios. *Energy Proced.* 4, 2253–2260.
- Witlox, H.W.M., Harper, M., Oke, A., 2012. Phast validation of discharge and atmospheric dispersion for carbon dioxide releases. In: Proc. 15th Annual Symposium, Mary Kay O'Connor Process Safety Centre, Texas A&M University, College Station, Texas, USA, 23–25 October 2012.
- Woolley, R.M., Fairweather, M., Wareing, C.J., Falle, S.A.E.G., Proust, C., Hebrard, J., Jamois, D., 2013. Experimental measurement and Reynolds-averaged Navier-Stokes modelling of the near-field structure of multi-phase CO₂ jet releases. *Int. J. Greenh. Gas Control* 18, 139–149.